SCIENCE CHINA
Information Sciences

• RESEARCH PAPER •

May 2022, Vol. 65 152202:1–152202:15
https://doi.org/10.1007/s11432-020-3205-4

Noncertainty-equivalent observer-based noncooperative target tracking control for unmanned aerial vehicles

Kenan YONG, Mou CHEN* & Qingxian WU

College of Automation Engineering, Nanjing University of Aeronautics and Astronautics, Nanjing 210016, *China*

Received 26 October 2020/Revised 27 December 2020/Accepted 2 February 2021/Published online 31 March 2022

Abstract Target tracking is a typical and challenging scenario that is required to be executed by unmanned aerial vehicles (UAVs) in operational environments. This work investigates the noncooperative target tracking control problem for UAVs. An integrated model is constructed by combining the dynamics of both the line-of-sight variables and the acceleration components. Particularly, the dynamics of the acceleration components, that contain unmeasurable states, characterize the relative motion between the noncooperative target and the UAV. To estimate these states, a globally convergent observer is developed by utilizing the noncertainty-equivalent (NCE) structure. With the integrated model and the NCE observer, an output-feedback target tracking control scheme is proposed using the dynamic surface control technique and the prescribed performance control method. Based on the Lyapunov approach, the relative spatial positions of the target and the UAV are proved to always stay within a specified operation region and ultimately converge to a small terminal region. Finally, simulation results are presented to illustrate the effectiveness of the proposed target tracking control scheme.

Keywords noncooperative target tracking, unmanned aerial vehicles, noncertainty-equivalent observer, prescribed performance control

Citation Yong K N, Chen M, Wu Q X. Noncertainty-equivalent observer-based noncooperative target tracking control for unmanned aerial vehicles. Sci China Inf Sci, 2022, 65(5): 152202, https://doi.org/10.1007/s11432-020-3205-4

1 Introduction

Target tracking is one of the fundamental missions for the unmanned aerial vehicle (UAV) with abundant applications such as securing, monitoring, and localizing an object of interest [1, 2]. Generally, the objective is to make the trajectory of the UAV follow that of a target while maintaining the standoff distance and the particular spatial relationship in the three-dimensional (3D) environment.

To achieve this objective, the target tracking mission has been extensively studied as the trajectory tracking problem [3–5] or the coordinated standoff problem [6, 7]. Nevertheless, the dynamics (e.g., acceleration) of the target are always assumed to be known or invariant, which may be unrealistic for the noncooperative target in practice. Recently, the improvement of target tracking performance has received considerable attention, especially in the case of the noncooperative target. To handle the unknown dynamics of the noncooperative target, there are numerous advanced approaches available in the research literature. For example, Oliveira et al. [8] introduced and investigated the moving path following problem to achieve single and multiple target tracking goals. In the report by Song et al. [9], the target behavior was reconstructed using the artificial neural network technique. All those aforementioned studies concentrate on the development of the guidance law via assuming that responses of the UAV dynamics are ideal [10]. However, the dynamics of UAV play a crucial role in the target tracking problem, and this requires further investigation.

Typically, through adjusting the torques acting on the UAV to rotate attitude angles, the flight control system makes the acceleration of the UAV coincide with the command signal generated by the target

* Corresponding author (email: chenmou@nuaa.edu.cn)

tracking control scheme [11]. Although the flight control system is designed to achieve significant acceleration tracking performance, the behavior of the UAV dynamics cannot be the same as that of the command signal [12]. Consequently, the aforementioned assumption regarding the responses of the UAV dynamics may not always be satisfied for the target tracking problem. Therefore, it is necessary to consider the dynamics of the UAV synthetically. In a similar direction, results have been reported for the target interception problem from the perspective of integrated guidance and control (IGC) scheme [13–16]. However, such target interception problems are quite distinct from the target tracking one because the target might process the close maneuverability with the UAV. Thus, any approach which neglects the dynamics of either the target or the UAV is unlikely to improve optimal target tracking performance.

A promising approach to tackle the target tracking problem is to directly study the relative dynamics between the target and the UAV. Because the states of the relative dynamics become unavailable owing to the noncooperative target, they should be estimated before exploring this approach further. Notably, as an advanced estimation methodology, the noncertainty-equivalent (NCE) structure has attracted significant attention. Using this structure, the estimator provides only a partial estimation of signals as required, and the full estimation is obtained by joining the partial estimation with a judiciously designed auxiliary nonlinear function of available signals. Accordingly, having benefited from the NCE structure, the estimator possesses the reduced-order design without estimating the available signals. Specifically, the popular nonlinear disturbance observer proposed by Chen et al. [17] is one of the typical NCE estimation methods that has been widely applied [18–20] and comprehensively investigated [21–23]. Alternatively, the immersion and invariance (I&I) technique reported by Astolfi et al. [24] provides another estimation method using the NCE structure. In this way, Karagiannis et al. [25] gave out the original theoretical guideline to design the NCE observer. Nevertheless, it is still difficult to provide a universal form of the NCE observer for the general nonlinear system [26,27], and thus the focused estimation problem deserves further investigation with respect to the relative dynamics.

Moreover, the target tracking problem also requires the relative distance and the spatial relationship to satisfy some constraints for escaping avoidance. In this regard, the prescribed performance control (PPC) method, proposed by Bechlioulis et al. [28], is a remarkable method that has been widely applied in practice to achieve the constrained control objective [29–31], and there have been a few reports of the PPC method being applied to the IGC scheme. By following this approach, in the report by An et al. [32], the PPC-based IGC scheme was designed for hypersonic flight vehicles which achieved fault-tolerant capability as well. The PPC-based adaptive IGC scheme reported by Liu et al. [33] was developed for a skid-to-turn missile by taking the input saturation and the state constraints into consideration. In light of all of these features, the PPC method is capable of being further developed for the target tracking problem to avoid escaping of the target.

Motivated by the above discussions, an output-feedback target tracking control scheme based on the NCE observer and PPC is developed for UAVs. The main contributions are summarized as follows: (1) An integrated model is constructed by combining the dynamics of both the line-of-sight (LOS) variables and the acceleration components. Particularly, the dynamics of acceleration components, that contain unmeasurable states, characterize the relative motion between the noncooperative target and the UAV. (2) The reduced-order nonlinear observer is developed to estimate the acceleration components without estimating the LOS variables. Based on the NCE structure, global convergence is achieved through exploiting the structure of the specific integrated model. Meanwhile, by tactfully choosing the internal variables and auxiliary nonlinear functions, this observer possesses a key property of the linearity of estimation error dynamics, and this property makes the analysis of the stability and the performance much more convenience. (3) The output-feedback target tracking control scheme is proposed with the integrated model and the NCE observer. Through synthesizing the PPC method and the dynamic surface control (DSC) technique, this scheme is capable of avoiding the escaping of the target; meanwhile, the LOS variables ultimately converge to a user-specified terminal region. (4) The theoretical condition is established after ensuring the scheme's feasibility and closed-loop stability. By selecting the parameters in this way, we prove that all the signals of the closed-loop system would be bounded and stay in a reasonable region. Accordingly, this condition provides a useful tool for control design and performance analysis in practical implementations.

The layout of this paper is as follows. The integrated model and the problem formulation are given in Section 2. The target tracking control scheme is presented in Section 3. The stability analysis and the theoretical condition are provided in Section 4. The numerical simulation results are included in Section 5. Finally, the conclusion is drawn in Section 6.

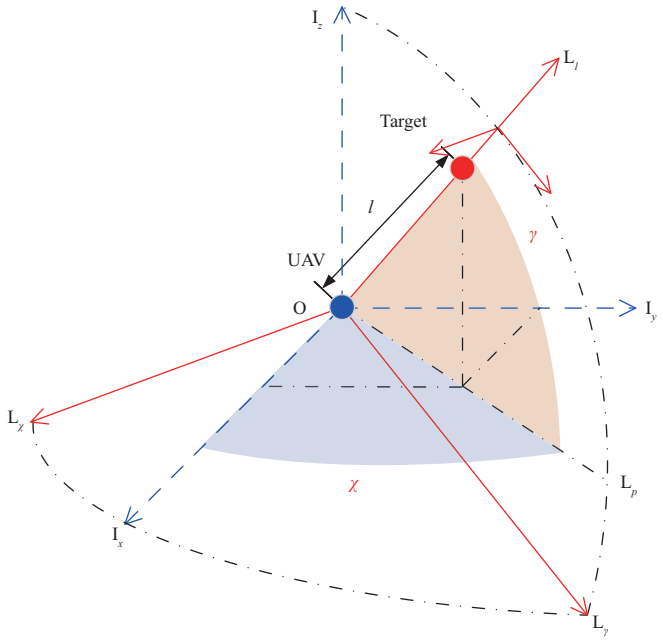

Figure 1 (Color online) The three-dimensional tracking geometry.

Notations. Throughout this paper, $\mathbb{R}$ stands for the real number set, and $\mathbb{R}^n$ respects n-dimensional Euclidean space. The symbol $\mathbb{I}_{j:i}$ with integers $i > j \geqslant 0$ denotes the set $\{j, j+1, \ldots, i-1, i\}$. For a real symmetrical matrix $\boldsymbol{Q}$, $\boldsymbol{Q} \succ 0$ means that $\boldsymbol{Q}$ is a positive definite matrix, and $\boldsymbol{Q} \prec 0$ denotes that $\boldsymbol{Q}$ is a negative definite one. $\boldsymbol{I}_n$ and $\boldsymbol{0}_n$ are the $n \times n$ identity and zero matrices, respectively. $\lambda_{\max}(\boldsymbol{Q})$ and $\lambda_{\min}(\boldsymbol{Q})$ represent the maximal and minimal eigenvalues of a given matrix $\boldsymbol{Q}$, respectively.

2 Integrated model and problem formulations

In this section, the relative relative dynamics, that are between the target and UAV, are established in the spherical LOS frame and the reference inertial frame. Then, by combining them together, the resulted nonlinear system leads to the integrated model. Accordingly, the target tracking problem is formulated.

2.1 Dynamics of LOS variables

To construct the relative dynamics, the noncooperative target and UAV are assumed to be two point masses in the 3D environment. With the given reference inertial frame $\mathcal{F}\{\mathrm{OI}_x\mathrm{I}_y\mathrm{I}_z\}$ that is attached to the body of the UAV and the line from the UAV to the target, the LOS frame $\mathcal{F}\{\mathrm{OL}_l\mathrm{L}_\chi\mathrm{L}_\gamma\}$ is defined with the spherical frame transformation. The 3D tracking geometry is shown in Figure 1, where the blue and red points denote the UAV and the target, respectively. In this LOS frame, the variables consist of the standoff distance l between the target and UAV, the azimuth angle χ from the inertial axis $\{\mathrm{OI}_x\}$ to the projection $\{\mathrm{OL}_p\}$ (the LOS axis $\{\mathrm{OL}_l\}$ onto the $\{\mathrm{OI}_x\mathrm{I}_y\}$ plane), and the elevation angle γ from the LOS axis $\{\mathrm{OL}_l\}$ to the $\{\mathrm{OI}_x\mathrm{I}_y\}$ plane. Accordingly, these LOS variables are defined with the components of the reference inertial frame as $l = \|\boldsymbol{p}_{tv}\|$, $\gamma = \mathrm{atan}(p_{tv}^y/p_{tv}^x)$, $\chi = \mathrm{atan}(p_{tv}^z/\sqrt{(p_{tv}^x)^2 + (p_{tv}^y)^2})$ where $\boldsymbol{p}_{tv} = [p_{tv}^x, p_{tv}^y, p_{tv}^z]^{\mathrm{T}}$ denotes the relative position vector of the noncooperative target with respect to the UAV in the reference inertial frame.

Then, under the conditions $l > 0$, $|\chi| < \pi/2$, and $|\gamma| < \pi/2$, the LOS dynamics is represented by the following nonlinear differential equations [34]:

$$\ddot{l} - l\dot{\gamma}^2 - l\dot{\chi}^2\cos^2\gamma = a_l,\ l\ddot{\chi}\cos\gamma + 2\dot{l}\dot{\chi}\cos\gamma - 2l\dot{\gamma}\dot{\chi}\sin\gamma = a_\chi,\ l\ddot{\gamma} + 2\dot{l}\dot{\gamma} + l\dot{\chi}^2\cos\gamma\sin\gamma = a_\gamma, \tag{1}$$

where $\boldsymbol{a}_{\mathrm{L}} = [a_l, a_\chi, a_\gamma]^{\mathrm{T}}$ is the relative acceleration between the target and UAV under the LOS frame,

and it is computed by

$$\boldsymbol{a}_{\mathrm{L}} = \begin{bmatrix} \cos\gamma\cos\chi & \cos\gamma\sin\chi & \sin\gamma \\ -\sin\chi & \cos\chi & 0 \\ -\sin\gamma\cos\chi & -\sin\gamma\sin\chi & \cos\gamma \end{bmatrix} (\boldsymbol{a}_t - \boldsymbol{a}_v),$$

where $\boldsymbol{a}_t, \boldsymbol{a}_v \in \mathbb{R}^3$ stand for the accelerations of the noncooperative target and UAV with respective to the reference inertial frame, respectively.

Remarkably, the existence of the mentioned conditions on l, χ, and γ is caused by the spherical frame transformation rather than the natural boundedness. In fact, due to limitations of the mission requirement (e.g., escaping avoidance) and the detection device (e.g., measurable range and visible angles), the required constraints on LOS variables are much stricter than the ones required by the LOS dynamics (1). For example, the escaping would happen when the azimuth angle χ or the elevation angle γ is larger than the visible angles or the standoff distance l is larger than the measurable range. Consequently, for all $t \geqslant 0$, the LOS variables are required to stay within an operation region $\mathcal{Y}_r$, i.e., $(l, \chi, \gamma) \in \mathcal{Y}_r$, and this region is defined as

$$\mathcal{Y}_r \triangleq \{\bar{l}_{\min} < l(t) < \bar{l}_{\max}, |\chi(t)| < \bar{\chi}, |\gamma(t)| < \bar{\gamma}\}, \tag{2}$$

where $0 < \bar{l}_{\min} < \bar{l}_{\max}$, $0 < \bar{\chi} \leqslant \pi/2$, and $0 < \bar{\gamma} \leqslant \pi/2$ are the user-specified constants.

Remark 1. It should be pointed out that the reference inertial frame is not a commonly used one, e.g., the north-east-down frame, and this frame is specified by the user and and keeps the stationary mapping relationship with the commonly used one. Since the spherical LOS frame is workable only in the half-space above the plane $p_v^x = 0$ of the reference inertial frame, users could eliminate this limitation through specifying an appropriate reference inertial frame according to the mission requirement. Specifically, the axis $\{\mathrm{OI}_x\}$ should be parallel to the line from the desired relative spatial position pointing to the target.

2.2 Dynamics of acceleration components

Generally speaking, the UAV dynamics contains two-fold, that is, (1) the UAV changes torques to rotate attitude angles and then to adjust the acceleration direction, and (2) it increases/decreases forces to enlarge/reduce the acceleration magnitude. To focus on the target tracking problem, we neglect the complicated nonlinearities of the rotational motion and suppose that the UAV is equipped with an inner-loop flight control system. Accordingly, this flight system can drive the acceleration $\boldsymbol{a}_v$ of the UAV to track the command $\boldsymbol{u} \in \mathbb{R}^3$, and then the resulted UAV dynamics is supposed to be a second-order low-pass filter as [16]

$$\ddot{\boldsymbol{a}}_v + \boldsymbol{C}_2\dot{\boldsymbol{a}}_v + \boldsymbol{C}_1\boldsymbol{a}_v = \boldsymbol{C}_1\boldsymbol{u}, \tag{3}$$

where $\boldsymbol{C}_1, \boldsymbol{C}_2 \in \mathbb{R}^{3\times3}$ are known constant matrices that determine the tracking performance of the flight control system.

On the other hand, if the target is another UAV, the UAV would share the similar responses of the dynamics with those of the target during the tracking process. Under this consideration, even though the noncooperative target dynamics is totally unknown, we can suppose that it owns the same form as the resulted UAV dynamics (3). Let $\boldsymbol{x}_{r,1} = \boldsymbol{a}_t - \boldsymbol{a}_v$, and then the relative dynamics between the target and UAV is formed as

$$\dot{\boldsymbol{x}}_{r,1} = \boldsymbol{x}_{r,2}, \quad \dot{\boldsymbol{x}}_{r,2} = -\boldsymbol{C}_1\boldsymbol{x}_{r,1} - \boldsymbol{C}_2\boldsymbol{x}_{r,2} - \boldsymbol{C}_1\boldsymbol{C}_1\boldsymbol{u} + \boldsymbol{d}, \tag{4}$$

where $\boldsymbol{x}_{r,1}, \boldsymbol{x}_{r,2} \in \mathbb{R}^3$ are the state vectors of the relative dynamics, and $\boldsymbol{d} \in \mathbb{R}^3$ is an unknown vector standing for the disagreement between the dynamics of the UAV and that of the target.

2.3 Problem formulation and preliminaries

In this work, the LOS variables l, χ, γ and their derivatives $\dot{l}$, $\dot{\chi}$, $\dot{\gamma}$ are assumed available by the measurement devices, e.g., the camera and the laser-radar. Meanwhile, to simultaneously consider the dynamics of both the target and the UAV, we prefer to investigate the relative dynamics (4). Since the tracked

target is a noncooperative one, its acceleration $\boldsymbol{a}_t$ is unavailable. Consequently, the states $\boldsymbol{x}_{r,1}$ and $\boldsymbol{x}_{r,2}$ of the relative dynamics also become unavailable, even though the ones $\boldsymbol{a}_v$ and $\dot{\boldsymbol{a}}_v$ of the UAV dynamics could be available.

Overall, define state vectors $\boldsymbol{x}_1 = [l, \chi, \gamma]^{\mathrm{T}}$, $\boldsymbol{x}_2 = \dot{\boldsymbol{x}}_1$, $\boldsymbol{x}_3 = \boldsymbol{x}_{r,1}$, and $\boldsymbol{x}_4 = \boldsymbol{x}_{r,2}$. Through taking into account the LOS dynamics (1) and the relative dynamics (4), the resulted system is organized as

$$\dot{\boldsymbol{x}}_1 = \boldsymbol{x}_2, \quad \dot{\boldsymbol{x}}_2 = \boldsymbol{F}(\boldsymbol{x}_1, \boldsymbol{x}_2) + \boldsymbol{G}(\boldsymbol{x}_1)\boldsymbol{x}_3, \quad \dot{\boldsymbol{x}}_3 = \boldsymbol{x}_4, \quad \dot{\boldsymbol{x}}_4 = -\boldsymbol{C}_1(\boldsymbol{x}_3 + \boldsymbol{u}) - \boldsymbol{C}_2\boldsymbol{x}_4 + \boldsymbol{d}, \tag{5}$$

where $\boldsymbol{y}_m = [\boldsymbol{x}_1^{\mathrm{T}}, \boldsymbol{x}_2^{\mathrm{T}}]^{\mathrm{T}}$ and $\boldsymbol{y}_c = \boldsymbol{x}_1$ are the measured and controlled output vectors, respectively, $\boldsymbol{F}: \mathbb{R}^3 \times \mathbb{R}^3 \to \mathbb{R}^3$ and $\boldsymbol{G}: \mathbb{R}^3 \to \mathbb{R}^{3\times 3}$ are the known function vector and matrix given in the form of

$$\boldsymbol{G}(\boldsymbol{x}_1) = \frac{1}{l}\begin{bmatrix} l\cos\gamma\cos\chi & l\cos\gamma\sin\chi & l\sin\gamma \\ -\sec\gamma\sin\chi & \sec\gamma\cos\chi & 0 \\ -\sin\gamma\cos\chi & -\sin\gamma\sin\chi & \cos\gamma \end{bmatrix}, \quad \boldsymbol{F}(\boldsymbol{x}_1, \boldsymbol{x}_2) = \frac{1}{l}\begin{bmatrix} l^2\dot{\gamma}^2 + l^2\dot{\chi}^2\cos^2\gamma \\ -2\dot{l}\dot{\chi} + 2l\dot{\gamma}\dot{\chi}\tan\gamma \\ -2\dot{l}\dot{\gamma} - l\dot{\chi}^2\cos\gamma\sin\gamma \end{bmatrix}.$$

Control objectives. Design an output-feedback target tracking control law for the nonlinear system (5) such that (1) the controlled output vector $\boldsymbol{y}_c$ is stabilized to a given constant vector $\boldsymbol{y}_r = [l_r, \chi_r, \gamma_r]^{\mathrm{T}} \in \mathcal{Y}_r$; (2) the stabilizing error vector $\boldsymbol{\epsilon} = [\epsilon_l, \epsilon_\chi, \epsilon_\gamma]^{\mathrm{T}} = \boldsymbol{y}_c - \boldsymbol{y}_r$ ultimately stays within the specified terminal region $\mathcal{E}_\infty \triangleq \{|\epsilon_i(t)| < \epsilon_i^\infty, i \in \{l, \chi, \gamma\}\}$ with user-specified constants $\epsilon_l^\infty, \epsilon_\chi^\infty, \epsilon_\gamma^\infty > 0$, i.e., $\boldsymbol{\epsilon}(t) \in \mathcal{E}_\infty, t \to \infty$; (3) the LOS variables always stay within the operation region $\mathcal{Y}_r$ defined in (2), i.e., $\boldsymbol{y}_c \in \mathcal{Y}_r, \forall t \geqslant 0$; (4) all the signals of the closed-loop system are bounded and stay in a reasonable region.

To proceed with the design of the control scheme, the following assumptions are required.

Assumption 1. The initial conditions of the UAV states are bounded. Meanwhile, there exists a positive constant vector $\boldsymbol{\epsilon}_0 = [\epsilon_l^0, \epsilon_\chi^0, \epsilon_\gamma^0]$ to make $\boldsymbol{x}_1(0)$ satisfy inequalities $\bar{l}_{\min} + \epsilon_l^0 < l(0) < \bar{l}_{\max} - \epsilon_l^0$, $|\chi(0)| < \bar{\chi} - \epsilon_\chi^0$, and $|\gamma(0)| < \bar{\gamma} - \epsilon_\gamma^0$.

Assumption 2. All the corresponding elements of the LOS variables belonging to the terminal region $\mathcal{E}_\infty$ are included in the operation region $\mathcal{Y}_r$, i.e., $\mathcal{E}_\infty \subset \{\bar{\boldsymbol{\epsilon}} \in \mathbb{R}^3 | \bar{\boldsymbol{\epsilon}} + \boldsymbol{y}_r \in \mathcal{Y}_r\}$.

Assumption 3 ([15])**.** For all $t \geqslant 0$, the acceleration $\boldsymbol{a}_t$ of the noncooperative target is bounded. Meanwhile, the disagreement between the dynamics of the UAV and the one of the target is also bounded, that is, there exists an unknown constant $\delta_d > 0$ to satisfy $\|\boldsymbol{d}\| \leqslant \delta_d$.

Remark 2. It is worthy noting that all those four goals correspond to the practical requirements of the target tracking problem. Objectives (1) and (2) allow users to determine the desired relative positions of the UAV with respect to the target and to specify the tracking performance of the UAV, respectively. Objectives (3) and (4) are essential requirements by accounting for the detection devices, the security consideration, and the UAV maneuverability.

3 NCE observer-based target tracking scheme

In this section, by designing the enclosing reference signal and specifying the boundary functions, the four objectives are unified as a single one that is to guarantee the boundedness of some transformed variables. Meanwhile, the NCE observer is developed to estimate the states of the relative dynamics. Accordingly, the output-feedback target tracking control scheme is proposed for the nonlinear system (5).

3.1 Control objective unification

To accomplish the ultimate goal of stabilizing $\boldsymbol{\epsilon}$, the target enclosing process should be taken into consideration, and it concentrates on guiding the UAV how to minimize relative distance within physical constraints of the UAV, such as the limitations on the velocity and attitude angles [4].

According to [4] and [35], the enclosing reference signal $\boldsymbol{y}_g(t) = [l_g, \chi_g, \gamma_g]^{\mathrm{T}}$ is generated by

$$\dot{\boldsymbol{y}}_g = -\boldsymbol{K}_1^g \mathbf{Tanh}\left(\boldsymbol{K}_2^g(\boldsymbol{y}_g - \boldsymbol{y}_r)\right), \quad \boldsymbol{y}_g(0) = \boldsymbol{y}_c(0), \tag{6}$$

where $\boldsymbol{K}_1^g, \boldsymbol{K}_2^g \succ 0$ are two designed matrices, and $\mathbf{Tanh}(\cdot) = [\tanh(\cdot), \tanh(\cdot), \tanh(\cdot)]^{\mathrm{T}}$ is the hyperbolic tangent function vector. Obviously, by choosing appropriate matrices $\boldsymbol{K}_1^g$ and $\boldsymbol{K}_2^g$, the enclosing reference signal $\boldsymbol{y}_g$ can always stay in the operation region $\mathcal{Y}_r$, i.e., $\boldsymbol{y}_g(t) \in \mathcal{Y}_r$, $\forall t \geqslant 0$, and $\boldsymbol{y}_g$

will asymptotically converge to $\boldsymbol{y}_r$, i.e., $\boldsymbol{y}_g(t) \to \boldsymbol{y}_r$ as $t \to \infty$. Meanwhile, differentiating $\dot{\boldsymbol{y}}_g$ yields $\ddot{\boldsymbol{y}}_g = -\boldsymbol{K}_1^g \mathbf{Sech}\left(\boldsymbol{K}_2^g(\boldsymbol{y}_g - \boldsymbol{y}_r)\right)\boldsymbol{K}_2^g \dot{\boldsymbol{y}}_g$ where $\mathbf{Sech}(\cdot) = \mathrm{diag}\{\mathrm{sech}(\cdot), \mathrm{sech}(\cdot), \mathrm{sech}(\cdot)\}$ is the hyperbolic secant function matrix. In light of the boundedness of $\mathbf{Tanh}(\cdot)$ and $\mathbf{Sech}(\cdot)$, the first-order and second-order derivatives of $\boldsymbol{y}_g$ are effectively limited, that is, there exist a constant $\delta_g > 0$ to satisfy $\boldsymbol{Y}_g^{\mathrm{T}}\boldsymbol{Y}_g \leqslant \delta_g$ with $\boldsymbol{Y}_g = [\boldsymbol{y}_g^{\mathrm{T}}, \dot{\boldsymbol{y}}_g^{\mathrm{T}}, \ddot{\boldsymbol{y}}_g^{\mathrm{T}}]^{\mathrm{T}}$. Based on these properties, objectives (1) and (4) are transformed to make the controlled output vector $\boldsymbol{y}_c$ track the enclosing reference signal $\boldsymbol{y}_g$.

Follow the goal that $\boldsymbol{y}_c$ tracks $\boldsymbol{y}_g$, and define the tracking error vector $\boldsymbol{e} = [e_l, e_\chi, e_\gamma]^{\mathrm{T}} = \boldsymbol{y}_c - \boldsymbol{y}_g$. To simultaneously unify objectives (2), (3), and the one that $\boldsymbol{y}_c$ tracks $\boldsymbol{y}_g$, $\boldsymbol{e}$ is expected to satisfy the following time-varying constraints:

$$\epsilon_i^l(t) < e_i < \epsilon_i^u(t),\ i \in \{l, \chi, \gamma\}, \tag{7}$$

where $\boldsymbol{\epsilon}_u = [\epsilon_l^u, \epsilon_\chi^u, \epsilon_\gamma^u]^{\mathrm{T}}$ and $\boldsymbol{\epsilon}_l = [\epsilon_l^l, \epsilon_\chi^l, \epsilon_\gamma^l]^{\mathrm{T}}$ are specified upper and lower boundary function vectors that denote the prescribed performance on $\boldsymbol{e}$. By considering desired constraints in objectives (2), (3) and initial conditions in Assumption 1, these specified boundary functions are specified as [28]

$$\dot{\epsilon}_i^u = -\Gamma_i^u(\epsilon_i^u - \epsilon_i^\infty),\ \epsilon_i^u(0) = \epsilon_i^0 \quad \text{and} \quad \dot{\epsilon}_i^l = -\Gamma_i^l(\epsilon_i^l + \epsilon_i^\infty),\ \epsilon_i^l(0) = -\epsilon_i^0, \tag{8}$$

where $i \in \{l, \chi, \gamma\}$, $\Gamma_i^u, \Gamma_i^l > 0$ are the designed parameters, ϵ_l^0, ϵ_χ^0, and ϵ_γ^0 are given in Assumption 1, moreover, ϵ_l^∞, ϵ_χ^∞, and ϵ_γ^∞ are the user-specified constants given in the control objective.

Of course, for each $i \in \{l, \chi, \gamma\}$, the specified boundary functions ϵ_i^u and ϵ_i^l would exponentially converge to ϵ_i^∞ and $-\epsilon_i^\infty$, respectively. Through choosing appropriate parameters Γ_i^u, Γ_i^l, $i \in \{l, \chi, \gamma\}$, we can make the following inequalities:

$$\begin{cases} \bar{l}_{\min} - l_g(t) \leqslant \epsilon_l^l(t) < 0 < \epsilon_l^u(t) \leqslant \bar{l}_{\max} - l_g(t), \\ -\bar{\chi} - \chi_g(t) \leqslant \epsilon_\chi^l(t) < 0 < \epsilon_\chi^u(t) \leqslant \bar{\chi} - \chi_g(t), \\ -\bar{\gamma} - \gamma_g(t) \leqslant \epsilon_\gamma^l(t) < 0 < \epsilon_\gamma^u(t) \leqslant \bar{\gamma} - \gamma_g(t) \end{cases} \tag{9}$$

hold for all $t \geqslant 0$ based on Assumption 2. In other words, objectives (2), (3), and the one that $\boldsymbol{y}_c$ tracks $\boldsymbol{y}_g$ are accomplished simultaneously if the constraints in (7) are guaranteed. Meanwhile, through differentiating (8), we get $\ddot{\epsilon}_i^j = -\Gamma_i^u \dot{\epsilon}_i^j$, $i \in \{l, \chi, \gamma\}$, $j \in \{u, l\}$, and then there exists another constant $\delta_\epsilon > 0$ to satisfy $\boldsymbol{Y}_\epsilon^{\mathrm{T}}\boldsymbol{Y}_\epsilon \leqslant \delta_\epsilon$ with $\boldsymbol{Y}_\epsilon = [\boldsymbol{\epsilon}_u^{\mathrm{T}}, \dot{\boldsymbol{\epsilon}}_u^{\mathrm{T}}, \ddot{\boldsymbol{\epsilon}}_u^{\mathrm{T}}, \boldsymbol{\epsilon}_l^{\mathrm{T}}, \dot{\boldsymbol{\epsilon}}_l^{\mathrm{T}}, \ddot{\boldsymbol{\epsilon}}_l^{\mathrm{T}}]^{\mathrm{T}}$. Accordingly, the introducing of these boundary function vectors would not destroy the boundedness of the closed-loop system. Namely, objectives (4) is fulfilled.

To accomplish the satisfaction of the constraints in (7), the error transformation function (ETF) in the PPC method is introduced here. Then, each constrained error variable e_i is transformed into an unconstrained one z_i by [28]

$$e_i - 0.5\left(\epsilon_i^u + \epsilon_i^l\right) = 0.5\left(\epsilon_i^u - \epsilon_i^l\right)\Xi(z_i),\ i \in \{l, \chi, \gamma\}, \tag{10}$$

where $\Xi(\cdot)$ is the ETF satisfying the following conditions [28]: (1) $\Xi(\cdot) \in \mathcal{C}^\infty$, $\partial\Xi(z_i)/\partial z_i > 0$, (2) $-1 < \Xi(z_i) < 1$, $-\infty < z_i < \infty$, and (3) $\lim_{z_i \to \infty}\Xi(z_i) = 1$, $\lim_{z_i \to -\infty}\Xi(z_i) = -1$.

Accordingly, the bounded transformed variable z_i can ensure the corresponding constraint on the error variable e_i with $i \in \{l, \chi, \gamma\}$. Let $\boldsymbol{z}_1 = [z_l, z_\chi, z_\gamma]^{\mathrm{T}}$. Considering (5), (10) and differentiating $\boldsymbol{z}_1$ yield

$$\dot{\boldsymbol{z}}_1 = \boldsymbol{\Omega}\boldsymbol{x}_2 + \boldsymbol{\Theta}, \tag{11}$$

where $\boldsymbol{\Omega} = \frac{\partial \boldsymbol{z}_1}{\partial \boldsymbol{e}}$ and $\boldsymbol{\Theta} = \frac{\partial \boldsymbol{z}_1}{\partial \boldsymbol{\epsilon}_u}\dot{\boldsymbol{\epsilon}}_u + \frac{\partial \boldsymbol{z}_1}{\partial \boldsymbol{\epsilon}_l}\dot{\boldsymbol{\epsilon}}_l - \frac{\partial \boldsymbol{z}_1}{\partial \boldsymbol{e}}\dot{\boldsymbol{y}}_g$ are the known matrix and vector, respectively.

As a result, the control objective is transformed to design an output-feedback control law to ensure $\boldsymbol{z}_1$ bounded. For the sake of notational simplicity, the symbols in bracket are omitted for $\boldsymbol{\Omega}$, $\boldsymbol{\Theta}$, $\boldsymbol{F}$, and $\boldsymbol{G}$ in the following presentation, except when it is noted for emphasis.

3.2 NCE observer

To estimate the unavailable state vectors $\boldsymbol{x}_3$ and $\boldsymbol{x}_4$ in the nonlinear system (5), the NCE observer that achieves the global convergence is developed in this subsection. Through exploiting the auxiliary nonlinear functions in the NCE structure, the observer possesses a linear error dynamics.

Based on the NCE structure, define two internal variable vectors as follows [36]:

$$\boldsymbol{s}_1 = \boldsymbol{x}_3 - \boldsymbol{L}_1(\boldsymbol{y}_m), \quad \boldsymbol{s}_2 = \boldsymbol{x}_4 - \boldsymbol{L}_2(\boldsymbol{y}_m), \tag{12}$$

where $\boldsymbol{L}_1 : \mathbb{R}^6 \to \mathbb{R}^3$ and $\boldsymbol{L}_2 : \mathbb{R}^6 \times \mathbb{R}^3 \to \mathbb{R}^3$ are the designed auxiliary nonlinear function vectors, and $\boldsymbol{y}_m$ is the measured output defined below the nonlinear system (5). Typically, the internal variable vectors are constructed for the unknown disturbances or parameters in the system dynamics. Here, they are associated with the unavailable states $\boldsymbol{x}_3$ and $\boldsymbol{x}_4$.

By taking into account the nonlinear system (5), the derivatives of $\boldsymbol{s}_1$ and $\boldsymbol{s}_2$ are written as

$$\dot{\boldsymbol{s}}_1 = \boldsymbol{x}_4 - \boldsymbol{L}_1^{x_2}\boldsymbol{G}\boldsymbol{x}_3 - \boldsymbol{L}_1^{x_1}\boldsymbol{x}_2 - \boldsymbol{L}_1^{x_2}\boldsymbol{F}, \ \dot{\boldsymbol{s}}_2 = -\boldsymbol{C}_1\boldsymbol{x}_3 - \boldsymbol{C}_2\boldsymbol{x}_4 - \boldsymbol{L}_2^{x_2}\boldsymbol{G}\boldsymbol{x}_3 + \boldsymbol{d} - \boldsymbol{L}_2^{x_1}\boldsymbol{x}_2 - \boldsymbol{L}_2^{x_2}\boldsymbol{F} - \boldsymbol{C}_1\boldsymbol{u}, \tag{13}$$

where $\boldsymbol{L}_j^{x_i} = \partial \boldsymbol{L}_j / \partial \boldsymbol{x}_i$, $i, j \in \mathbb{I}_{1:2}$ are the known nonlinear function matrices.

Through introducing (12) into (13), we have

$$\dot{\boldsymbol{s}}_1 = -\boldsymbol{L}_1^{x_2}\boldsymbol{G}\boldsymbol{s}_1 + \boldsymbol{s}_2 + \boldsymbol{\Psi}_1, \quad \dot{\boldsymbol{s}}_2 = -\boldsymbol{L}_2^{x_2}\boldsymbol{G}\boldsymbol{s}_1 - \boldsymbol{C}_1\boldsymbol{s}_1 - \boldsymbol{C}_2\boldsymbol{s}_2 + \boldsymbol{\Psi}_2 + \boldsymbol{d}, \tag{14}$$

where $\boldsymbol{\Psi}_1 = \boldsymbol{L}_2 - \boldsymbol{L}_1^{x_2}\boldsymbol{G}\boldsymbol{L}_1 - \boldsymbol{L}_1^{x_1}\boldsymbol{x}_2 - \boldsymbol{L}_1^{x_2}\boldsymbol{F}$ and $\boldsymbol{\Psi}_2 = -\boldsymbol{C}_1(\boldsymbol{L}_1 + \boldsymbol{u}) - \boldsymbol{C}_2\boldsymbol{L}_2 - \boldsymbol{L}_2^{x_1}\boldsymbol{x}_2 - \boldsymbol{L}_2^{x_2}(\boldsymbol{G}\boldsymbol{L}_1 + \boldsymbol{F})$ are the known function vectors.

For the convenience of the parameter selection and the stability analysis, we prefer to construct the nonlinear function matrices $\boldsymbol{L}_1^{x_2}\boldsymbol{G}$ and $\boldsymbol{L}_2^{x_2}\boldsymbol{G}$ to be linear. Without loss of generality, the nonlinear function vectors $\boldsymbol{L}_1$ and $\boldsymbol{L}_2$ are designed in the form of $\boldsymbol{L}_1(\boldsymbol{y}_m) = \boldsymbol{S}_1\boldsymbol{G}^{-1}\boldsymbol{x}_2$ and $\boldsymbol{L}_2(\boldsymbol{y}_m) = \boldsymbol{S}_2\boldsymbol{G}^{-1}\boldsymbol{x}_2$ where $\boldsymbol{S}_1, \boldsymbol{S}_2 \in \mathbb{R}^{3\times 3}$ are two designed constant matrices.

It is clear that $\boldsymbol{L}_1^{x_1}$ and $\boldsymbol{L}_2^{x_1}$ are known. Meanwhile, $\boldsymbol{L}_1^{x_2}$ and $\boldsymbol{L}_2^{x_2}$ are written as $\boldsymbol{L}_1^{x_2} = \boldsymbol{S}_1\boldsymbol{G}^{-1}$ and $\boldsymbol{L}_2^{x_2} = \boldsymbol{S}_2\boldsymbol{G}^{-1}$, respectively. The differential equations (14) are reorganized as

$$\dot{\boldsymbol{s}} = \boldsymbol{A}\boldsymbol{s} + \boldsymbol{\Psi} + \boldsymbol{B}\boldsymbol{d} \tag{15}$$

with $\boldsymbol{s} = [\boldsymbol{s}_1^{\mathrm{T}}, \boldsymbol{s}_2^{\mathrm{T}}]^{\mathrm{T}}$, $\boldsymbol{\Psi} = [\boldsymbol{\Psi}_1^{\mathrm{T}}, \boldsymbol{\Psi}_2^{\mathrm{T}}]^{\mathrm{T}}$, $\boldsymbol{B} = [\boldsymbol{0}_3, \boldsymbol{I}_3]^{\mathrm{T}}$, and $\boldsymbol{A} = [-\boldsymbol{S}_1, \boldsymbol{I}_3; -\boldsymbol{C}_1 - \boldsymbol{S}_2, -\boldsymbol{C}_2]$.

Then, the estimations of $\boldsymbol{x}_3$ and $\boldsymbol{x}_4$ are achieved by designing the Luenberger observer for $\boldsymbol{s}$. Accordingly, the estimator $\hat{\boldsymbol{s}}$ and the outputs $\hat{\boldsymbol{x}}_3$, $\hat{\boldsymbol{x}}_4$ are designed as follows:

$$\dot{\hat{\boldsymbol{s}}} = \boldsymbol{A}\hat{\boldsymbol{s}} + \boldsymbol{\Psi}, \ \hat{\boldsymbol{x}}_3 = \hat{\boldsymbol{s}}_1 + \boldsymbol{L}_1, \ \hat{\boldsymbol{x}}_4 = \hat{\boldsymbol{s}}_2 + \boldsymbol{L}_2, \tag{16}$$

where $\hat{\boldsymbol{s}} = [\hat{\boldsymbol{s}}_1^{\mathrm{T}}, \hat{\boldsymbol{s}}_2^{\mathrm{T}}]^{\mathrm{T}}$, $\hat{\boldsymbol{s}}_1, \hat{\boldsymbol{s}}_2 \in \mathbb{R}^3$ are the estimations of $\boldsymbol{s}_1$ and $\boldsymbol{s}_2$, respectively. It is remarkable that the estimated variables $\hat{\boldsymbol{s}}_1$ and $\hat{\boldsymbol{s}}_2$ are only partial estimations of the unknown states $\boldsymbol{x}_3$ and $\boldsymbol{x}_4$. The full estimations of $\boldsymbol{x}_3$ and $\boldsymbol{x}_4$ are obtained as (16) by joining the partial estimations with the designed auxiliary nonlinear functions $\boldsymbol{L}_1$ and $\boldsymbol{L}_2$.

Furthermore, to analyze the stability of the NCE observer, define the estimation error vector $\boldsymbol{z}_s = \hat{\boldsymbol{s}} - \boldsymbol{s}$. Consider (15) and (16), and the dynamics of $\boldsymbol{z}_s$ is obtained as $\dot{\boldsymbol{z}}_s = \boldsymbol{A}\boldsymbol{z}_s - \boldsymbol{B}\boldsymbol{d}$ which means that the estimation convergence depends on the matrix $\boldsymbol{A}$. Choose the Lyapunov function candidate as $V_s = \boldsymbol{z}_s^{\mathrm{T}}\boldsymbol{P}\boldsymbol{z}_s$ where $\boldsymbol{P} \succ 0$ is a designed matrix, and there exists another matrix $\bar{\boldsymbol{P}}$ to satisfy $\boldsymbol{P} = \bar{\boldsymbol{P}}^{\mathrm{T}}\bar{\boldsymbol{P}}$ under the Cholesky decomposition. Applying $\|\boldsymbol{d}\| \leqslant \delta_d$ in Assumption 3, and differentiating V_s yield

$$\dot{V}_s \leqslant \boldsymbol{z}_s^{\mathrm{T}}\boldsymbol{\Lambda}\boldsymbol{z}_s - 0.5\boldsymbol{z}_s^{\mathrm{T}}\boldsymbol{z}_s/\eta_s + \delta_d^2/\eta_s, \tag{17}$$

where $\boldsymbol{\Lambda} = \boldsymbol{P}\boldsymbol{A} + \boldsymbol{A}^{\mathrm{T}}\boldsymbol{P} + \eta_s\boldsymbol{P}\boldsymbol{P} + 0.5\boldsymbol{I}_6/\eta_s$, and η_s is a designed parameter. Meanwhile, through considering (12) and (16), we also have the estimation error vectors $\tilde{\boldsymbol{x}}_3 = \hat{\boldsymbol{x}}_3 - \boldsymbol{x}_3$ and $\tilde{\boldsymbol{x}}_4 = \hat{\boldsymbol{x}}_4 - \boldsymbol{x}_4$ as which indicates that $\tilde{\boldsymbol{x}}_3$ and $\tilde{\boldsymbol{x}}_4$ are equivalent to $\boldsymbol{z}_s$, i.e., $\boldsymbol{z}_s = [\tilde{\boldsymbol{x}}_3^{\mathrm{T}}, \tilde{\boldsymbol{x}}_4^{\mathrm{T}}]^{\mathrm{T}}$.

Apparently, according to the bounded stability theory, the estimation error vectors $\tilde{\boldsymbol{x}}_3$ and $\tilde{\boldsymbol{x}}_4$ are guaranteed bounded if $\boldsymbol{\Lambda} \prec 0$. It is easy to achieve $\boldsymbol{\Lambda} \prec 0$ via choosing the appropriate matrices $\boldsymbol{S}_1$ and $\boldsymbol{S}_2$. We will explore the stability of the closed-loop system in Section 4.

3.3 Target tracking control design

With the ETF and the NCE observer, the target tracking control scheme is developed by utilizing the DSC technique in this subsection.

Through integrating (11) and (16), the nonlinear system (5) with unavailable states and constrained states is rewritten as

$$\begin{cases} \dot{\boldsymbol{z}}_1 = \boldsymbol{\Omega}\boldsymbol{x}_2 + \boldsymbol{\Theta},\ \dot{\boldsymbol{x}}_2 = \boldsymbol{F} + \boldsymbol{G}(\hat{\boldsymbol{s}}_1 + \boldsymbol{L}_1 + \tilde{\boldsymbol{x}}_3), \\ \dot{\hat{\boldsymbol{s}}}_1 = -\boldsymbol{S}_1\hat{\boldsymbol{s}}_1 + \hat{\boldsymbol{s}}_2 + \boldsymbol{\Psi}_1,\ \dot{\hat{\boldsymbol{s}}}_2 = -(\boldsymbol{C}_1 + \boldsymbol{S}_2)\hat{\boldsymbol{s}}_1 - \boldsymbol{C}_2\hat{\boldsymbol{s}}_2 + \boldsymbol{\Psi}_2. \end{cases} \tag{18}$$

Apparently, the constrained state vector $\boldsymbol{x}_1$ is transformed to an unconstrained variable vector $\boldsymbol{z}_1$, the states $\boldsymbol{x}_3$ and $\boldsymbol{x}_4$ are replaced by the newly constructed states $\hat{\boldsymbol{s}}_1$ and $\hat{\boldsymbol{s}}_2$. Although the observer (16) is an NCE one, the rewritten nonlinear system (18) still satisfies the strict-feedback form. Therefore, the backstepping-derived technique such as DSC technique is applied to design the acceleration command of the UAV.

For convenience, the step-by-step designing procedure of the DSC technique is summarized as a whole. Define the tracking error vectors as

$$\boldsymbol{z}_2 = \boldsymbol{x}_2 - \boldsymbol{\xi}_2,\quad \boldsymbol{z}_3 = \hat{\boldsymbol{s}}_1 - \boldsymbol{\xi}_3,\quad \boldsymbol{z}_4 = \hat{\boldsymbol{s}}_2 - \boldsymbol{\xi}_4, \tag{19}$$

where $\boldsymbol{\xi}_i \in \mathbb{R}^3, i \in \mathbb{I}_{2:4}$ are the first-order filters. These filters are given in the form of

$$\tau_i\dot{\boldsymbol{\xi}}_i + \boldsymbol{\xi}_i = \boldsymbol{\xi}_i^*,\quad \boldsymbol{\xi}_i(0) = \boldsymbol{\xi}_i^*(0), \tag{20}$$

where $i \in \mathbb{I}_{2:4}$, $\tau_i \in \mathbb{R}$ are three designed time constants, and $\boldsymbol{\xi}_i^* \in \mathbb{R}^3$ are the virtual control laws that will be designed later soon in (22).

By considering (18) and defining the filter error vectors $\tilde{\boldsymbol{\xi}}_i = \boldsymbol{\xi}_i - \boldsymbol{\xi}_i^*$, $i \in \mathbb{I}_{2:4}$, the dynamics of the error vectors $\boldsymbol{z}_i$, $i \in \mathbb{I}_{1:4}$ are written as

$$\begin{cases} \dot{\boldsymbol{z}}_1 = \boldsymbol{\Omega}(\boldsymbol{\xi}_2^* + \tilde{\boldsymbol{\xi}}_2 + \boldsymbol{z}_2) + \boldsymbol{\Theta},\ \dot{\boldsymbol{z}}_2 = \boldsymbol{F} + \boldsymbol{G}(\boldsymbol{\xi}_3^* + \tilde{\boldsymbol{\xi}}_3 + \boldsymbol{z}_3 + \tilde{\boldsymbol{x}}_3) + \boldsymbol{G}\boldsymbol{L}_1 - \dot{\boldsymbol{\xi}}_2, \\ \dot{\boldsymbol{z}}_3 = -\boldsymbol{S}_1\hat{\boldsymbol{s}}_1 + (\boldsymbol{\xi}_4^* + \tilde{\boldsymbol{\xi}}_4 + \boldsymbol{z}_4) + \boldsymbol{\Psi}_1 - \dot{\boldsymbol{\xi}}_3,\ \dot{\boldsymbol{z}}_4 = -(\boldsymbol{C}_1 + \boldsymbol{S}_2)\hat{\boldsymbol{s}}_1 - \boldsymbol{C}_2\hat{\boldsymbol{s}}_2 + \boldsymbol{\Psi}_2 - \dot{\boldsymbol{\xi}}_4. \end{cases} \tag{21}$$

Since the actual control input $\boldsymbol{u}$ is included in the known function vector $\boldsymbol{\Psi}_2$ by recalling (14), we regard $\boldsymbol{\Psi}_2$ as another virtual control input, and the command signals $\boldsymbol{u}$ of the UAV acceleration will be given out later soon in (23). Accordingly, these virtual control laws are designed as

$$\begin{cases} \boldsymbol{\xi}_2^* = -\boldsymbol{\Omega}^{-1}(\boldsymbol{K}_1\boldsymbol{z}_1 + \boldsymbol{\Theta}) - \eta_1\boldsymbol{\Omega}\boldsymbol{z}_1, \\ \boldsymbol{\xi}_3^* = -\boldsymbol{G}^{-1}(\boldsymbol{K}_2\boldsymbol{z}_2 + \boldsymbol{F} + \boldsymbol{\Omega}\boldsymbol{z}_1 - \dot{\boldsymbol{\xi}}_2) - 0.5(\eta_2 + \eta_s)\boldsymbol{G}^{\mathrm{T}}\boldsymbol{z}_2 - \boldsymbol{L}_1, \\ \boldsymbol{\xi}_4^* = -\boldsymbol{K}_3\boldsymbol{z}_3 + \dot{\boldsymbol{\xi}}_3 - \boldsymbol{G}^{\mathrm{T}}\boldsymbol{z}_2 - \eta_3\boldsymbol{z}_3 + \boldsymbol{S}_1\hat{\boldsymbol{s}}_1 - \boldsymbol{\Psi}_1, \\ \boldsymbol{\Psi}_2 = -\boldsymbol{K}_4\boldsymbol{z}_4 - \boldsymbol{z}_3 + (\boldsymbol{C}_1 + \boldsymbol{S}_1)\hat{\boldsymbol{s}}_1 + \boldsymbol{C}_2\hat{\boldsymbol{s}}_2 + \dot{\boldsymbol{\xi}}_4, \end{cases} \tag{22}$$

where $\boldsymbol{K}_i \succ 0$, $i \in \mathbb{I}_{1:4}$ and $\eta_i > 0$, $i \in \mathbb{I}_{1:3}$ are four designed matrices and three designed parameters, respectively, and η_s is defined below (17). Accordingly, with the virtual control law $\boldsymbol{\Psi}_2$, the command signal vector of the UAV acceleration is computed as

$$\boldsymbol{u} = \boldsymbol{C}_1^{-1}\big(-\boldsymbol{C}_1\hat{\boldsymbol{x}}_3 - \boldsymbol{C}_2\hat{\boldsymbol{x}}_4 - \boldsymbol{L}_2^{x_2}\boldsymbol{G}\boldsymbol{L}_1 - \boldsymbol{L}_2^{x_1}\boldsymbol{x}_2 - \boldsymbol{L}_2^{x_2}\boldsymbol{F} + \boldsymbol{K}_4\boldsymbol{z}_4 - \boldsymbol{S}_1\hat{\boldsymbol{s}}_1 - \dot{\boldsymbol{\xi}}_4 + \boldsymbol{z}_3\big). \tag{23}$$

Remark 3. It is worthwhile to note that distinct from the existing IGC schemes in [13,15], the proposed scheme concentrates on the relative dynamics between the target and UAV seen from (1) and (4), and thus, the constructed scheme becomes an output-feedback one. Meanwhile, instead of directly employing the linear observer like [12, 16], the specifically designed nonlinear observer which possesses the linear dynamics (17) of estimation errors is developed via utilizing the NCE structure. Furthermore, through proposing additional constraints (9) on the parameters of the boundary functions, the well-developed PPC method, e.g., [33], is synthesized in the target tracking control scheme to further accomplish the escaping avoidance of the target.

4 Stability analysis and main result

In this section, the main result of the proposed target tracking control scheme is summarized in terms of the theoretical proof. Furthermore, a guidance on parameter selection is provided for practical implementations.

Substituting (22) into (21) yields $\dot{\boldsymbol{z}}_1 = -\boldsymbol{K}_1\boldsymbol{z}_1 - \eta_1\boldsymbol{\Omega}\boldsymbol{\Omega}\boldsymbol{z}_1 + \boldsymbol{\Omega}(\boldsymbol{z}_2 + \tilde{\boldsymbol{\xi}}_2)$, $\dot{\boldsymbol{z}}_2 = -\boldsymbol{K}_2\boldsymbol{z}_2 - \boldsymbol{\Omega}\boldsymbol{z}_1 - 0.5(\eta_2 + \eta_s)\boldsymbol{G}\boldsymbol{G}^{\mathrm{T}}\boldsymbol{z}_2 + \boldsymbol{G}(\boldsymbol{z}_3 + \tilde{\boldsymbol{x}}_3 + \tilde{\boldsymbol{\xi}}_3)$, $\dot{\boldsymbol{z}}_3 = -\boldsymbol{K}_3\boldsymbol{z}_3 - \boldsymbol{G}^{\mathrm{T}}\boldsymbol{z}_2 - \eta_3\boldsymbol{z}_3 + (\boldsymbol{z}_4 + \tilde{\boldsymbol{\xi}}_4)$, and $\dot{\boldsymbol{z}}_4 = -\boldsymbol{K}_4\boldsymbol{z}_4 - \boldsymbol{z}_3$. Choose the Lyapunov function as $V_z = 0.5\sum_{i=1}^{4}\boldsymbol{z}_i^{\mathrm{T}}\boldsymbol{z}_i$. Differentiating V_z and applying the Young's inequality yield

$$\dot{V}_z \leqslant -\sum_{i=1}^{4}\boldsymbol{z}_i^{\mathrm{T}}\boldsymbol{K}_i\boldsymbol{z}_i + 0.5\tilde{\boldsymbol{x}}_3^{\mathrm{T}}\tilde{\boldsymbol{x}}_3/\eta_s + \sum_{i=2}^{4}0.5\tilde{\boldsymbol{\xi}}_i^{\mathrm{T}}\tilde{\boldsymbol{\xi}}_i/\eta_{i-1}, \tag{24}$$

which means that if $\tilde{\boldsymbol{x}}_3$ and $\tilde{\boldsymbol{\xi}}_i$, $i \in \mathbb{I}_{2:4}$ are bounded, then V_z is bounded and the target tracking control law in (22) and (23) could accomplish the control objectives.

Now, we further consider the stability of the filter error vectors $\tilde{\boldsymbol{\xi}}_i$, $i \in \mathbb{I}_{2:4}$. Define the vectors $\boldsymbol{\upsilon}_1 = [\boldsymbol{d}^{\mathrm{T}}, \boldsymbol{Y}_g^{\mathrm{T}}, \boldsymbol{Y}_\epsilon^{\mathrm{T}}]^{\mathrm{T}}$ and $\boldsymbol{\upsilon}_i = [\sqrt{2}(\bar{\boldsymbol{P}}\boldsymbol{z}_s)^{\mathrm{T}}, \boldsymbol{z}_1^{\mathrm{T}}, \ldots, \boldsymbol{z}_i^{\mathrm{T}}, \tilde{\boldsymbol{\xi}}_2^{\mathrm{T}}, \ldots, \tilde{\boldsymbol{\xi}}_i^{\mathrm{T}}]^{\mathrm{T}}$ with $i \in \mathbb{I}_{2:4}$ and $\bar{\boldsymbol{P}}$ defined above (17). Through differentiating filter error vectors $\tilde{\boldsymbol{\xi}}_i, i \in \mathbb{I}_{2:4}$, we have

$$\dot{\tilde{\boldsymbol{\xi}}}_i = -\tilde{\boldsymbol{\xi}}_i/\tau_i - \boldsymbol{m}_i(\boldsymbol{\upsilon}_1, \boldsymbol{\upsilon}_i),\ i \in \mathbb{I}_{2:4}, \tag{25}$$

where $\boldsymbol{m}_i(\boldsymbol{\upsilon}_1, \boldsymbol{\upsilon}_i) = \frac{\partial\boldsymbol{\xi}_i^*}{\partial\boldsymbol{\epsilon}_u}\ddot{\boldsymbol{\epsilon}}_u + \frac{\partial\boldsymbol{\xi}_i^*}{\partial\boldsymbol{\epsilon}_l}\ddot{\boldsymbol{\epsilon}}_l + \frac{\partial\boldsymbol{\xi}_i^*}{\partial\boldsymbol{\epsilon}_u}\dot{\boldsymbol{\epsilon}}_u + \frac{\partial\boldsymbol{\xi}_i^*}{\partial\boldsymbol{\epsilon}_l}\dot{\boldsymbol{\epsilon}}_l + \frac{\partial\boldsymbol{\xi}_i^*}{\partial\boldsymbol{z}_s}\dot{\boldsymbol{z}}_s + \sum_{j=1}^{i-1}\frac{\partial\boldsymbol{\xi}_i^*}{\partial\boldsymbol{z}_j}\dot{\boldsymbol{z}}_j + \sum_{j=2}^{i-1}\frac{\partial\boldsymbol{\xi}_i^*}{\partial\tilde{\boldsymbol{\xi}}_j}\dot{\tilde{\boldsymbol{\xi}}}_j$, $i \in \mathbb{I}_{2:4}$ are continuous function vectors. According to Assumption 3, the inequalities $\boldsymbol{Y}_g^{\mathrm{T}}\boldsymbol{Y}_g \leqslant \delta_g$ below (6) and $\boldsymbol{Y}_\epsilon^{\mathrm{T}}\boldsymbol{Y}_\epsilon \leqslant \delta_\epsilon$ below (9), the compact set $\mathcal{P}_1 \triangleq \{\boldsymbol{\upsilon}_1 : \|\boldsymbol{\upsilon}_1\|^2 \leqslant \delta_d^2 + \delta_g + \delta_\epsilon\}$ is an invariant one. Due to the fact $\boldsymbol{\xi}_i(0) = \boldsymbol{\xi}_i^*(0)$ in (20), we obtain $\tilde{\boldsymbol{\xi}}_i(0) = 0$ for any $i \in \mathbb{I}_{2:4}$. As the initial conditions of the UAV states are supposed bounded in Assumption 1, the estimation error vector $\boldsymbol{z}_s$, the transformed variable vector $\boldsymbol{z}_1$, and the tracking error vector $\boldsymbol{z}_i$, $i \in \mathbb{I}_{2:4}$ are initially bounded. Without loss of generality, there exists a constant $p_0 > 0$ to make all the initial conditions satisfy

$$0.5\sum_{i=1}^{4}\boldsymbol{z}_i^{\mathrm{T}}(0)\boldsymbol{z}_i(0) + 0.5\sum_{i=2}^{4}\tilde{\boldsymbol{\xi}}_i^{\mathrm{T}}(0)\tilde{\boldsymbol{\xi}}_i(0) + \boldsymbol{z}_s^{\mathrm{T}}(0)\boldsymbol{P}\boldsymbol{z}_s(0) \leqslant p_0. \tag{26}$$

Then, for any given constants $p \geqslant p_0$, the sets $\mathcal{P}_i \triangleq \{\boldsymbol{\upsilon}_i : \|\boldsymbol{\upsilon}_i\|^2 \leqslant p\}$, $i \in \mathbb{I}_{2:4}$ are compact. Thus, the sets $\mathcal{P}_1 \times \mathcal{P}_i$, $i \in \mathbb{I}_{2:4}$ are also compact. With the continuous property of $\boldsymbol{m}_i$, there exist constants $\bar{M}_i > 0$, $i \in \mathbb{I}_{2:4}$ to satisfy

$$\|\boldsymbol{m}_i(\boldsymbol{\upsilon}_1, \boldsymbol{\upsilon}_i)\| \leqslant \bar{M}_i,\ \forall(\boldsymbol{\upsilon}_1, \boldsymbol{\upsilon}_i) \in \mathcal{P}_1 \times \mathcal{P}_i,\ i \in \mathbb{I}_{2:4}, \tag{27}$$

which indicates that the filter error vector could be bounded if the sets $\mathcal{P}_i$, $i \in \mathbb{I}_{2:4}$ are invariant. Overall, the control objective would be accomplished if $\mathcal{P}_4$ is invariant.

4.1 Main result

Let $\kappa = \min_{i\in\mathbb{I}_{1:4}, j\in\mathbb{I}_{2:4}}\{2\lambda_{\min}(\boldsymbol{K}_i), 0.5/\eta_{j-1} - 0.5\tau_j, \lambda_{\max}(\boldsymbol{\Lambda})/\lambda_{\max}(\boldsymbol{P})\}$, and $\bar{\delta} = \delta_d^2/\eta_s + 0.5\sum_{i=2}^{4}\bar{M}_i^2\tau_i$. With the design procedure and the provided insight, the main result of this paper is summarized in Theorem 1 for the noncooperative target tracking control problem of the UAV.

Theorem 1. Consider the integrated model (5) under Assumptions 1–3. Through choosing appropriate matrices $\boldsymbol{K}_1^g, \boldsymbol{K}_2^g$ and parameters Γ_i^u, Γ_i^l, $i \in \{l, \chi, \gamma\}$, the enclosing reference signal generated by (6) and the boundary functions specified in (8) satisfy the inequalities in (9). With the ETF in (10), the NCE observer (16), and the first-order filters (20), the DSC technique-based target tracking control law is designed according to (22) and (23). For any given constant $p \geqslant p_0$ with p_0 given in (26), if matrices $\boldsymbol{K}_i, i \in \mathbb{I}_{1:4}$, $\boldsymbol{S}_1$, $\boldsymbol{S}_2$, $\boldsymbol{P}$, and parameters η_s, η_i, $i \in \mathbb{I}_{1:3}$, τ_i, $i \in \mathbb{I}_{2:4}$ are designed to satisfy $-\kappa p + \bar{\delta} \leqslant 0$, then (1) the stabilizing error vector $\boldsymbol{\epsilon}$ ultimately stays within the specified terminal region $\mathcal{E}_\infty$, (2) the controlled output vector $\boldsymbol{y}_c$ always stays within the operation region $\mathcal{Y}_r$, and (3) all the signals of the closed-loop system are bounded.

Proof. Consider the stability of all the error vectors in $\boldsymbol{\upsilon}_4$, and the augmented Lyapunov function candidate is written as $V = 0.5\boldsymbol{\upsilon}_4^{\mathrm{T}}\boldsymbol{\upsilon}_4 = V_s + V_z + 0.5\sum_{i=2}^{4}\tilde{\boldsymbol{\xi}}_i^{\mathrm{T}}\tilde{\boldsymbol{\xi}}_i$. Invoke (17), (24), (25), and (27), and then for all $\boldsymbol{\upsilon}_4 \in \mathcal{P}_4$, the derivative of V satisfies

$$\dot{V} \leqslant \boldsymbol{z}_s^{\mathrm{T}}\boldsymbol{\Lambda}\boldsymbol{z}_s - \sum_{i=1}^{4}\boldsymbol{z}_i^{\mathrm{T}}\boldsymbol{K}_i\boldsymbol{z}_i + \sum_{i=2}^{4}0.5\tau_i\bar{M}_i^2 + 0.5\sum_{i=2}^{4}(1/\eta_{i-1} - 1/\tau_i)\,\tilde{\boldsymbol{\xi}}_i^{\mathrm{T}}\tilde{\boldsymbol{\xi}}_i + \delta_d^2/\eta_s \leqslant -\kappa V + \bar{\delta}. \tag{28}$$

Then, with the condition $-\kappa p+\bar{\delta}\leqslant 0$, we have $\dot{V}\leqslant 0$ on $V=p$ which means that the sets $\mathcal{P}_i$, $i\in\mathbb{I}_{2:4}$ are invariant. Associated with the initial condition in (26), we can conclude that the inequalities $V\leqslant p$, (27), and (28) hold for all $t\geqslant 0$. Thus, the estimation error vector $\boldsymbol{z}_s$, the transformed variable vector $\boldsymbol{z}_1$, the tracking error vectors $\boldsymbol{z}_i$, $i\in\mathbb{I}_{2:4}$, and the filter error vectors $\boldsymbol{\xi}_i$, $i\in\mathbb{I}_{2:4}$ are all bounded.

As the statement in Subsection 3.1, the controlled output vector $\boldsymbol{y}_c$ satisfies the constraints in (7) with the norm-bounded $\boldsymbol{z}_1$, and thus, the stabilizing error vector $\boldsymbol{\epsilon}$ ultimately stays within the specified terminal region $\mathcal{E}_\infty$. Through integrating the inequalities in (7) and (9), we can conclude that $\boldsymbol{y}_c\in\mathcal{Y}_r$, $\forall t\geqslant 0$. In light of the bounded V, we also know that all the states in the nonlinear system (21) are bounded which indicates the boundedness of the UAV states. In addition, since the designed nonlinear function vectors $\boldsymbol{L}_1$ and $\boldsymbol{L}_2$ are bounded, the auxiliary variable vectors $\boldsymbol{s}_1$ and $\boldsymbol{s}_2$ are bounded as well. Therefore, all the signals in the closed-loop system are bounded. This completes the proof.

4.2 Parameter selection and feasibility endurance

There are many designed matrices and parameters to be chosen in the proposed target tracking control scheme. In terms of their functionalities, a guideline for their design is provided for users in this subsection.

For the enclosing reference signal generated in (6) and the boundary functions specified in (8), the parameters contain $\boldsymbol{K}_1^g$, $\boldsymbol{K}_2^g$, Γ_i^u, and Γ_i^l with $i\in\{l,\chi,\gamma\}$. Specifically, the UAV will more rapidly enclose the target through increasing $\|\boldsymbol{K}_{g,1}\|$, but this increase would bring more load on the UAV dynamics. By appropriately selecting the off-diagonal elements of $\boldsymbol{K}_{g,2}$, the enclosing trajectory can be specified. Furthermore, under the satisfaction of the inequality conditions in (9), choosing larger Γ_i^u and Γ_i^l will result in better tracking performance of e_i with $i\in\{l,\chi,\gamma\}$.

On the other hand, $\boldsymbol{K}_i$, $i\in\mathbb{I}_{1:4}$, $\boldsymbol{S}_i$, $i\in\mathbb{I}_{1:2}$, and $1/\tau_i$, $i\in\mathbb{I}_{2:4}$ are the feedback gains of the control laws (22) and (23), the NCE observer (16), and the filters (25), respectively. Moreover, $\boldsymbol{P}$, η_s, and η_i are utilized to suppress the coupling between $\tilde{\boldsymbol{x}}_3$ and $\tilde{\boldsymbol{x}}_4$, the one between $\tilde{\boldsymbol{x}}_3$ and $\boldsymbol{z}_3$, and the one between $\boldsymbol{z}_i$ and $\tilde{\boldsymbol{\xi}}_{i+1}$, respectively. Choosing smaller $\lambda_{\max}(\boldsymbol{\Lambda})/\lambda_{\max}(\boldsymbol{P})$ and τ_i, $i\in\mathbb{I}_{2:4}$ will result in better estimation performance of the NCE observer and the corresponding filters, respectively. Meanwhile, the error variable vector $\boldsymbol{z}_i$ is decreased by increasing $\boldsymbol{K}_i$, $i\in\mathbb{I}_{1:4}$, η_s, and η_i, $i\in\mathbb{I}_{1:3}$, but these increases would bring a larger command signal of the UAV acceleration.

Notably, about the condition in $-\kappa p+\bar{\delta}\leqslant 0$, the user can somewhat decrease $\bar{\delta}$ by selecting subtly the parameters of the enclosing reference signal and the boundary functions, i.e., $\boldsymbol{K}_1^g$, $\boldsymbol{K}_2^g$, Γ_i^u, and Γ_i^l with $i\in\{l,\chi,\gamma\}$. In addition, through increasing $\lambda_{\min}(\boldsymbol{K}_i)$, $i\in\mathbb{I}_{1:4}$, η_s, η_i, $i\in\mathbb{I}_{1:3}$, τ_i, $i\in\mathbb{I}_{2:4}$, and $\lambda_{\max}(\boldsymbol{\Lambda})/\lambda_{\max}(\boldsymbol{P})$, the user can obtain a sufficiently larger κ which guarantees the existence of parameters, but this increase would also bring a heavier UAV load. Therefore, caution must be exercised in the selection of these parameters, due to the fact that there exists a trade-off between the control performance and other issues.

5 Numerical illustration

In this section, the extensive simulation studies are implemented to illustrate the effectiveness of the proposed target tracking control scheme in two practical cases, namely tracking the coordinated (non-maneuvering) and noncooperative (maneuvering) target. For rigorous verification, the proposed control scheme is compared with the proportional derivative (PD)-based and the PPC-based scheme.

5.1 Simulation description

Since the north-east-down frame, denoted as $\mathcal{F}\{\mathrm{OXYZ}\}$, is a commonly-used frame, it is employed as the actual inertial frame for convenience of implementation. The relationship between $\mathcal{F}\{\mathrm{OXYZ}\}$ and $\mathcal{F}\{\mathrm{OI}_x\mathrm{I}_y\mathrm{I}_z\}$ is described as $\{\mathrm{OI}_x\}\to\{\mathrm{OZ}\}$, $\{\mathrm{OI}_y\}\to\{\mathrm{OX}\}$, and $\{\mathrm{OI}_z\}\to\{\mathrm{OY}\}$.

About the nonlinear system (5), the parameters of the UAV dynamics are given as $\boldsymbol{C}_1=-10\boldsymbol{I}_3$ and $\boldsymbol{C}_2=-3\boldsymbol{I}_3$. The constants of the operation region $\mathcal{Y}_r$ defined in (2) are given by $l_{\min}=1$ m, $l_{\max}=150$ m, and $\bar{\chi}=\bar{\gamma}=60$ deg. The desired controlled output vector is given as $\boldsymbol{y}_r=[5\text{ m},0\text{ deg},0\text{ deg}]^{\mathrm{T}}$ with the terminal region specified by $\epsilon_l^\infty=5$ m, $\epsilon_\chi^\infty=2.5$ deg, $\epsilon_\gamma^\infty=2.5$ deg. The initial conditions of the LOS variables and the UAV dynamics are given as $\boldsymbol{x}_1(0)=[100\text{ m},40\text{ deg},50\text{ deg}]^{\mathrm{T}}$, $\boldsymbol{x}_2(0)=[-5\text{ m/s},-1\text{ deg/s},-1\text{ deg/s}]^{\mathrm{T}}$, $\boldsymbol{a}_v(0)=[0,0,0]^{\mathrm{T}}$ g, and $\dot{\boldsymbol{a}}_v(0)=[0,0,0]^{\mathrm{T}}$ g/s where "g" is the gravity acceleration. Accordingly, there exist constants $\epsilon_l^0=20$ m, $\epsilon_\chi^0=20$ deg, and $\epsilon_\gamma^0=20$ deg

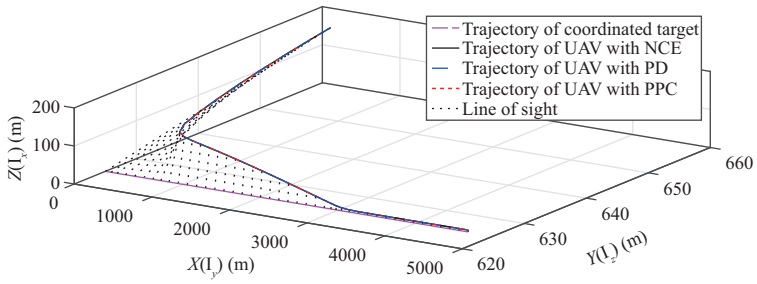

Figure 2 (Color online) Case 1: Trajectories of the UAV and the target.

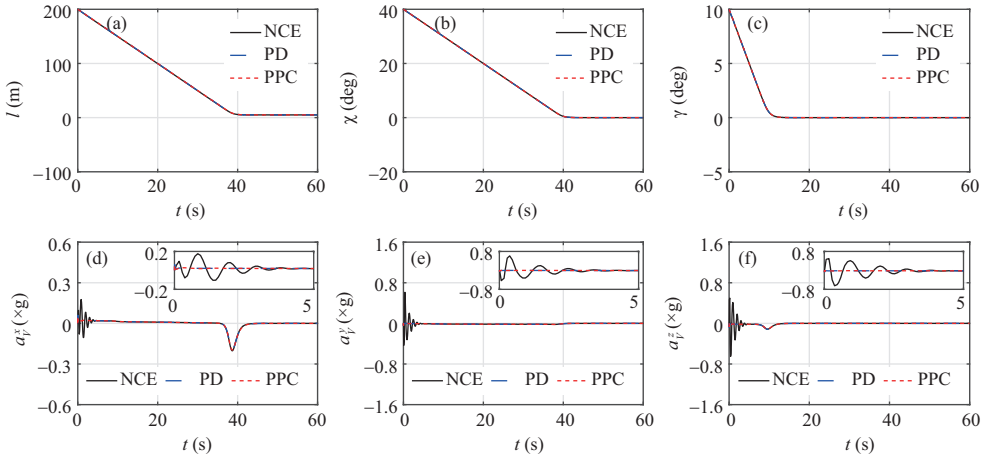

Figure 3 (Color online) Case 1: LOS variables (a)–(c) and UAV acceleration (d)–(f).

to satisfy Assumption 1. For the enclosing reference signal in (6), the matrices are designed as $\boldsymbol{K}_1^g = \mathrm{diag}\{5, 0.0175, 0.0175\}$, $\boldsymbol{K}_1^g = \boldsymbol{K}_2^{g-1}$. For the boundary functions in (8), the designed parameters are specified as $\Gamma_l^u = \Gamma_l^l = 0.22$, $\Gamma_\chi^u = \Gamma_\chi^l = 0.17$, and $\Gamma_\gamma^u = \Gamma_\gamma^l = 0.17$ which make the inequalities in (9) hold. For the NCE observer in (16), the designed matrices are given as $\boldsymbol{S}_1 = 20\boldsymbol{I}_3$ and $\boldsymbol{S}_2 = 20\boldsymbol{I}_3$. Moreover, the initial conditions of the NCE observer are given as $\hat{\boldsymbol{s}}_1(0) = \hat{\boldsymbol{s}}_2(0) = [-27, 80, 150]^{\mathrm{T}}$. The ETF in (10) is chosen as $\Xi(\cdot) = 2\arctan(\cdot)/\pi$. For the first-order filters, the time constants are chosen as $\tau_i = 1/300, i \in \mathbb{I}_{2:4}$. For the tracking control law given by (22) and (23), the parameters are designed as $\eta_1 = 0.05$, $\eta_2 = 10^{-3}$, $\eta_3 = 10$, and $\eta_s = 10^{-3}$. Moreover, the matrices are designed as $\boldsymbol{K}_1 = \mathrm{diag}\{3, 0.1, 0.1\}$, $\boldsymbol{K}_2 = \mathrm{diag}\{2.5, 0.5, 0.5\}$, $\boldsymbol{K}_3 = 10\boldsymbol{I}_3$, and $\boldsymbol{K}_4 = 20\boldsymbol{I}_4$.

For comparison, besides the control scheme developed in this paper, the PD-based and the PPC-based schemes are simulated. For the notational simplicity, the superscripts "d" and "p" denote the components of the PD-based and the PPC-based schemes, respectively. The PD-based scheme will use directly the error $\boldsymbol{e}$ to construct the control law, i.e., $\boldsymbol{z}_1^d = \boldsymbol{e}$. Likewise, the error transformation of the PPC-based scheme is designed as the same as (11), i.e., $\boldsymbol{z}_1^p = \boldsymbol{z}_1$. Similar with (19), (20), (22), and (23), the error vectors are defined as $\boldsymbol{z}_2^k = \boldsymbol{x}_2 - \boldsymbol{\xi}_2^k$, $\boldsymbol{z}_3^k = \boldsymbol{a}_v - \boldsymbol{\xi}_3^k$, and $\boldsymbol{z}_4^k = \dot{\boldsymbol{a}}_v - \boldsymbol{\xi}_4^k$ with $k \in \{d, p\}$. The filters $\boldsymbol{\xi}_i^k$ with $i \in \mathbb{I}_{2:4}$ and $k \in \{d, p\}$ of the DSC technique are specified in the form of $\tau_i^k \dot{\boldsymbol{\xi}}_i^k + \boldsymbol{\xi}_i^k = \boldsymbol{\xi}_i^{k*}$ with time constants τ_i^k and initial conditions $\boldsymbol{\xi}_i^k(0) = \boldsymbol{\xi}_i^{k*}(0)$. Moreover, the filter inputs $\boldsymbol{\xi}_i^{k*}$, $i \in \mathbb{I}_{2:4}$ are specified as $\boldsymbol{\xi}_2^{d*} = -\boldsymbol{K}_1^d \boldsymbol{z}_1^d + \dot{\boldsymbol{y}}_r - 0.5\eta_1^d \boldsymbol{z}_1^d$, $\boldsymbol{\xi}_3^{d*} = \boldsymbol{G}^{-1}(\boldsymbol{K}_2^d \boldsymbol{z}_2^d + \boldsymbol{F} + \boldsymbol{z}_1^d - \dot{\boldsymbol{\xi}}_2^d) + 0.5\eta_2^d \boldsymbol{G}^{\mathrm{T}} \boldsymbol{z}_2^d$, $\boldsymbol{\xi}_4^{d*} = -\boldsymbol{K}_3^d \boldsymbol{z}_3^d + \boldsymbol{G}^{\mathrm{T}} \boldsymbol{z}_2^d - \eta_3^d \boldsymbol{z}_3^d + \dot{\boldsymbol{\xi}}_3^d$, $\boldsymbol{\xi}_2^{p*} = -\boldsymbol{\Omega}^{-1}(\boldsymbol{K}_1^p \boldsymbol{z}_1^p + \boldsymbol{\Theta}) - 0.5\eta_1^p \boldsymbol{\Omega} \boldsymbol{z}_1^p$, $\boldsymbol{\xi}_3^{p*} = \boldsymbol{G}^{-1}(\boldsymbol{K}_2^p \boldsymbol{z}_2^p + \boldsymbol{F} + \boldsymbol{\Omega} \boldsymbol{z}_1^p - \dot{\boldsymbol{\xi}}_2^p) + 0.5\eta_2^p \boldsymbol{G}^{\mathrm{T}} \boldsymbol{z}_2^p$, $\boldsymbol{\xi}_4^{p*} = -\boldsymbol{K}_3^p \boldsymbol{z}_3^p + \boldsymbol{G}^{\mathrm{T}} \boldsymbol{z}_2^p - \eta_3^k \boldsymbol{z}_3^p + \dot{\boldsymbol{\xi}}_3^p$, and then the command signal vectors $\boldsymbol{u}^k, k \in \{d, p\}$ of both the PD-based and PPC-based schemes are designed in the form of $\boldsymbol{u}^k = \boldsymbol{C}_1^{-1}(-\boldsymbol{K}_4^k \boldsymbol{z}_4^k - \boldsymbol{z}_3^k + \dot{\boldsymbol{\xi}}_4^k + \boldsymbol{C}_1 \boldsymbol{a}_v + \boldsymbol{C}_2 \dot{\boldsymbol{a}}_v)$ where $\boldsymbol{K}_i^k$, $i \in \mathbb{I}_{1:4}$ are gain matrices and η_i^k, $i \in \mathbb{I}_{1:3}$ are tuning parameters with $k \in \{p, d\}$.

5.2 Simulation results

Case 1. For the case of tracking coordinated target, the target is supposed to move to an invariant direction with the uniform velocity. Consequently, the acceleration components are chosen as zeros, i.e., $\boldsymbol{a}_t = [0, 0, 0]^{\mathrm{T}}$. In this case, the performance of the PD-based and PPC-based schemes is tuned to be as

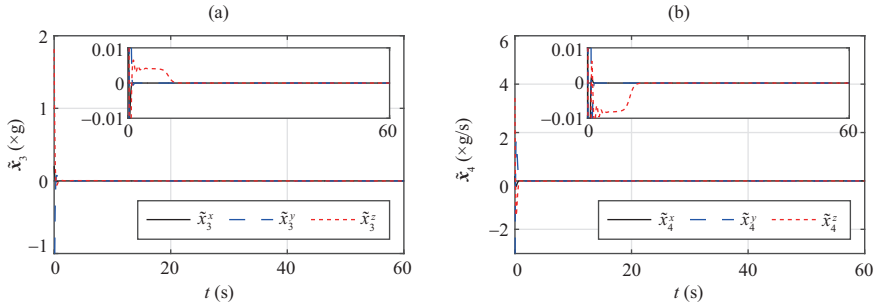

Figure 4 (Color online) Case 1: Estimation errors $\tilde{\boldsymbol{x}}_3 = [\tilde{x}_3^x, \tilde{x}_3^y, \tilde{x}_3^z]^{\mathrm{T}}$ (a) and $\tilde{\boldsymbol{x}}_4 = [\tilde{x}_4^x, \tilde{x}_4^y, \tilde{x}_4^z]^{\mathrm{T}}$ (b) of the NCE observer.

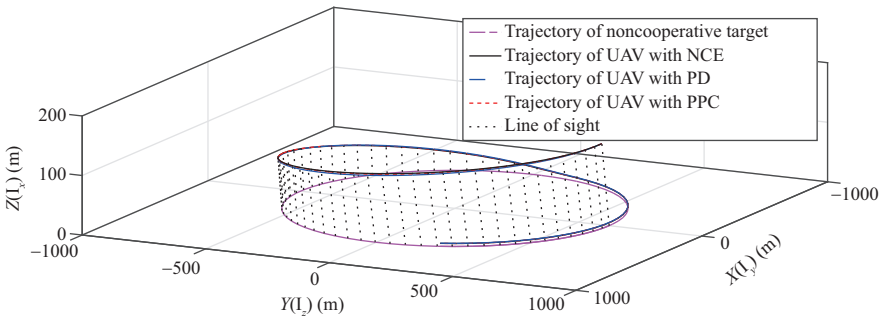

Figure 5 (Color online) Case 2: Trajectories of the UAV and the target.

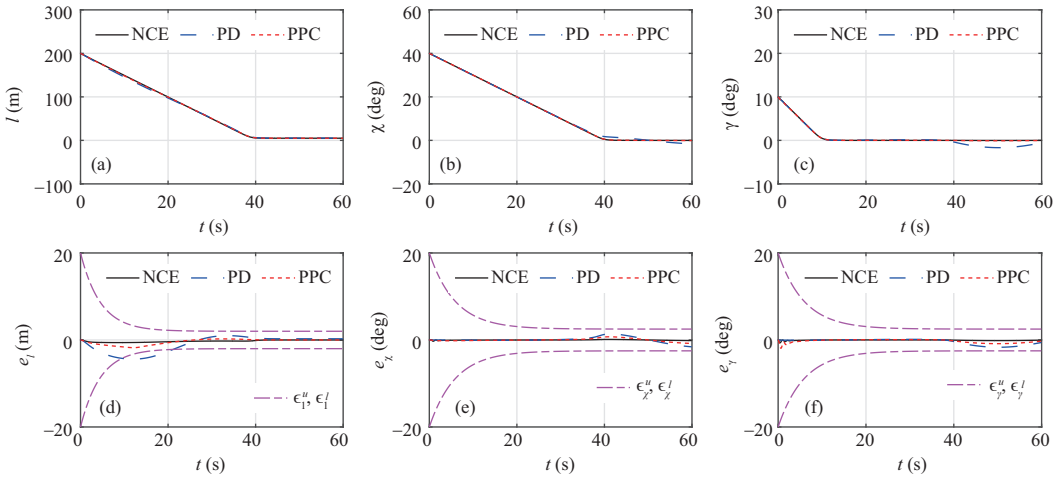

Figure 6 (Color online) Case 2: LOS variables (a)–(c) and their tracking errors (d)–(f).

close as possible to the proposed one by choosing appropriate parameters. Therefore, the corresponding parameters are chosen as $\boldsymbol{K}_i^p = \boldsymbol{K}_i$, $i \in \mathbb{I}_{1:4}$, $\boldsymbol{K}_1^d = \mathrm{diag}\{0.5, 7.5, 7.5\}$, $\boldsymbol{K}_2^d = \mathrm{diag}\{1, 8, 8\}$, $\boldsymbol{K}_i^d = \boldsymbol{K}_i$, $i \in \mathbb{I}_{3:4}$, $\eta_i^p = \eta_i$, $i \in \mathbb{I}_{1:3}$, $\eta_1^d = 1$, $\eta_2^d = 0.02$, $\eta_3^d = 10$, and $\tau_i^k = \tau_i$, $i \in \mathbb{I}_{1:3}$, $k \in \{d, p\}$.

The simulation results are presented in Figures 2–4. The trajectories of the UAV and the target are plotted in Figure 2, which reveals that all the compared schemes accomplish the coordinated target tracking objective. Figures 3(a)–(c) show that the stabilizing performance of $\boldsymbol{x}_1$ is almost the same for three compared schemes, which indicates the reasonability of the parameter selection for PD-based and PPC-based schemes. And, the responses of the UAV accelerations $\boldsymbol{a}_v = [a_v^x, a_v^y, a_v^z]^{\mathrm{T}}$ under those schemes are displayed in Figures 3(d)–(f). Notably, there exists short period oscillation for the UAV accelerations under the proposed scheme, while these accelerations are reasonable. It is due to the existence of the initial error for the NCE observer. As observed from Figures 4(a) and (b), the estimation error vectors $\tilde{\boldsymbol{x}}_3$ and $\tilde{\boldsymbol{x}}_4$ asymptotically converge to zero, respectively, and then the oscillation of the UAV acceleration is also converged.

Case 2. For the case of tracking the noncooperative target, the target trajectory in $\mathcal{F}\{\mathrm{OXYZ}\}$ frame

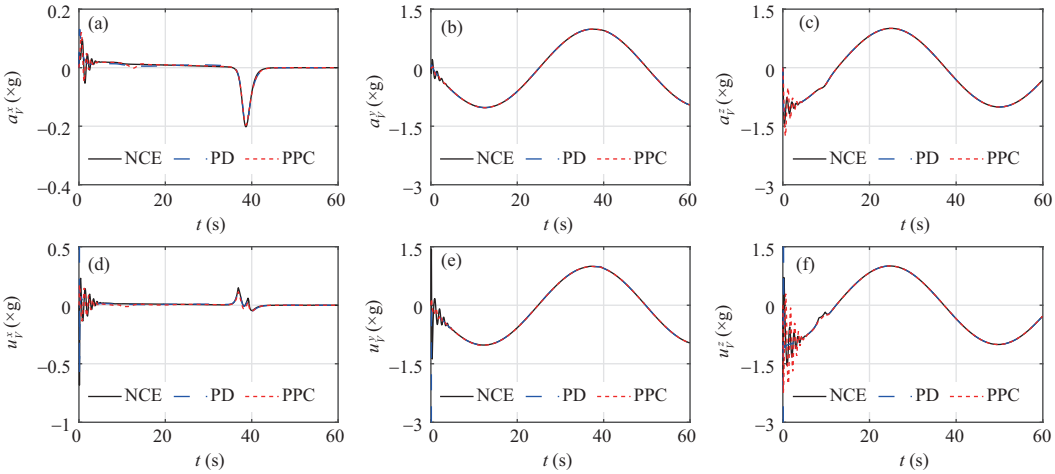

Figure 7 (Color online) Case 2: UAV acceleration (a)–(c) and control input (d)–(f).

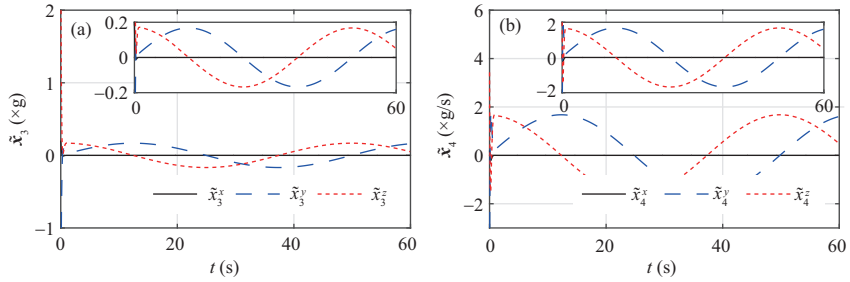

Figure 8 (Color online) Case 2: Estimation errors $\tilde{\boldsymbol{x}}_3 = [\tilde{x}_3^x, \tilde{x}_3^y, \tilde{x}_3^z]^{\mathrm{T}}$ (a) and $\tilde{\boldsymbol{x}}_4 = [\tilde{x}_4^x, \tilde{x}_4^y, \tilde{x}_4^z]^{\mathrm{T}}$ (b) of the NCE observer.

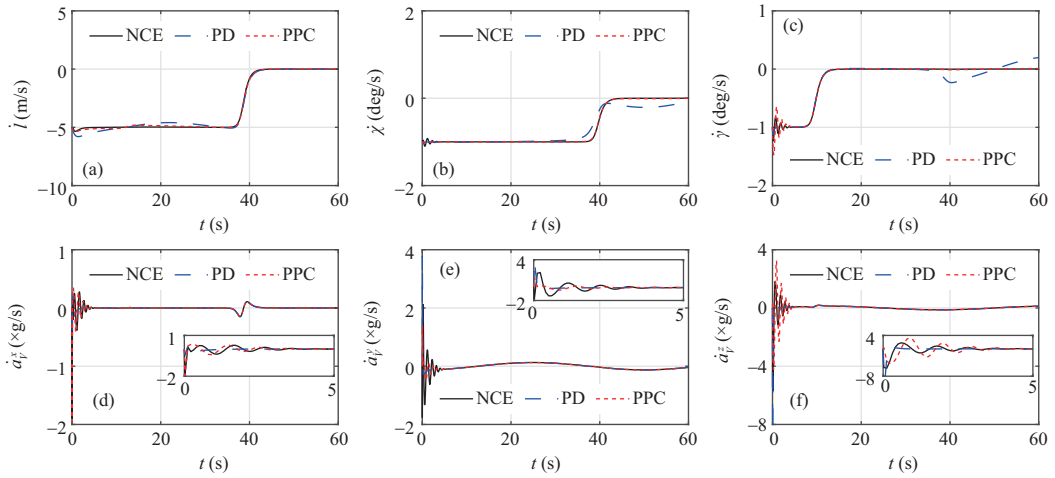

Figure 9 (Color online) Case 2: Derivatives of LOS variables (a)–(c) and UAV acceleration (d)–(f).

is given as $\mathrm{X}(t) = 625\sin(\pi t/25)$ m, $\mathrm{Y}(t) = 625\cos(\pi t/25)$ m, and $\mathrm{Z}(t) = 0$ m. The parameters of the compared schemes are chosen as the same as the former case.

The simulation results are shown in Figures 5–9. The trajectory of the target and those of the UAV under three schemes are shown in Figure 5. We observe that three schemes accomplish the noncooperative target tracking objective, simultaneously. The curves of $\boldsymbol{x}_1$ and $\boldsymbol{e}$ are plotted in Figures 6(a)–(c) and (d)–(f), respectively. It is seen that the stabilizing performance of the proposed scheme is also excellent like Case 1, whereas the PD-based scheme has poor stabilizing performance and that of the PPC-based one is just acceptable. Specifically, since e_l is sensitive to the initial state, i.e., $\boldsymbol{a}_t(0) - \boldsymbol{a}_v(0)$, the transient performance in Figure 6(d) is degraded for the UAV under the PD-based and the PPC-based schemes. The steady-state performance in Figures 6(e) and (f) becomes poor for two compared schemes, as the

impacts of $\boldsymbol{a}_t$ on e_χ and e_γ are increasing during the enclosing of the UAV and the target. Meanwhile, as seen from Figures 7(a)–(f), the short period oscillation appears for both the PD-based and PPC-based schemes and even larger than the proposed one. All the above distinct features of the proposed scheme are owing to the consideration of the relative dynamics and the reliable estimation of the NCE observer seen from Figures 8(a) and (b). Furthermore, the responses of the left closed-loop signals, i.e., $\boldsymbol{x}_2$ and $\dot{\boldsymbol{a}}_v$, are drawn in Figures 9(a)–(f), which indicates the boundedness of the closed-loop system.

Overall, the constraints on the standoff distance and the spatial relationship are guaranteed. The NCE observer is capable of well estimating the unavailable states of relative dynamics. All these ensure that the proposed target tracking control scheme fulfills the target tracking mission without resorting to the exact knowledge of the target dynamics.

6 Conclusion

The noncooperative target tracking control problem has been investigated for UAVs. By combining the dynamics of both the LOS variables and acceleration components, an integrated model has been constructed. To estimate the states of the relative dynamics, an NCE observer has been developed and global convergence has been achieved. With the outputs of the NCE observer, a target tracking control scheme has been proposed that utilizes both the DSC technique and the PPC method. It has been shown theocratically that the relative spatial positions of the target and the UAV always stay within a specified operation region and ultimately converge to a small terminal region. Finally, simulation results have been presented to illustrate the effectiveness of the proposed scheme.

Acknowledgements This work was supported in part by the National Science Fund (Grant No. 61825302, 62103188), in part by Key R&D Projects (Social Development) in Jiangsu Province of China (Grant No. BE2020704), and in part by Jiangsu Province "333" Project (Grant No. BRA2019051).

References

1 Lyu Y, Kang T N, Pan Q, et al. UAV sense and avoidance: concepts, technologies, and systems (in Chinese). Sci Sin Inform, 2019, 49: 520–537
2 Kim S, Oh H, Tsourdos A. Nonlinear model predictive coordinated standoff tracking of a moving ground vehicle. J Guid Control Dyn, 2013, 36: 557–566
3 Wang M, Zhang Y L, Dong H F, et al. Trajectory tracking control of a bionic robotic fish based on iterative learning. Sci China Inf Sci, 2020, 63: 170202
4 Yu X, Liu L. Target enclosing and trajectory tracking for a mobile robot with input disturbances. IEEE Control Syst Lett, 2017, 1: 221–226
5 Zhu P X, Ren W. Fully distributed joint localization and target tracking with mobile robot networks. IEEE Trans Contr Syst Technol, 2021, 29: 1519–1532
6 Frew E W, Lawrence D A, Morris S. Coordinated standoff tracking of moving targets using Lyapunov guidance vector fields. J Guid Control Dyn, 2008, 31: 290–306
7 Yoon S, Park S, Kim Y. Circular motion guidance law for coordinated standoff tracking of a moving target. IEEE Trans Aerosp Electron Syst, 2013, 49: 2440–2462
8 Oliveira T, Aguiar A P, Encarnacao P. Moving path following for unmanned aerial vehicles with applications to single and multiple target tracking problems. IEEE Trans Robot, 2016, 32: 1062–1078
9 Song Y D, Guo J X. Neuro-adaptive fault-tolerant tracking control of lagrange systems pursuing targets with unknown trajectory. IEEE Trans Ind Electron, 2017, 64: 3913–3920
10 Park S. Guidance law for standoff tracking of a moving object. J Guid Control Dyn, 2017, 40: 2948–2955
11 Yong K N, Chen M, Wu Q X. Immersion and invariance-based integrated guidance and control for unmanned aerial vehicle path following. Int J Syst Sci, 2019, 50: 1052–1068
12 Chwa D. Robust nonlinear disturbance observer based adaptive guidance law against uncertainties in missile dynamics and target maneuver. IEEE Trans Aerosp Electron Syst, 2018, 54: 1739–1749
13 Padhi R, Chawla C, Das P G. Partial integrated guidance and control of interceptors for high-speed ballistic targets. J Guid Control Dyn, 2014, 37: 149–163
14 Panchal B, Mate N, Talole S E. Continuous-time predictive control-based integrated guidance and control. J Guid Control Dyn, 2017, 40: 1579–1595
15 Chwa D, Choi J Y. Adaptive nonlinear guidance law considering control loop dynamics. IEEE Trans Aerosp Electron Syst, 2003, 39: 1134–1143
16 Chwa D, Choi J Y, Anavatti S G. Observer-based adaptive guidance law considering target uncertainties and control loop dynamics. IEEE Trans Control Syst Technol, 2006, 14: 112–123
17 Chen W H, Ballance D J, Gawthrop P J, et al. A nonlinear disturbance observer for robotic manipulators. IEEE Trans Ind Electron, 2000, 47: 932–938
18 Chen M. Constrained control allocation for overactuated aircraft using a neurodynamic model. IEEE Trans Syst Man Cybern Syst, 2016, 46: 1630–1641
19 Zhang C, Chen Z J, Wei C. Sliding mode disturbance observer-based backstepping control for a transport aircraft. Sci China Inf Sci, 2014, 57: 052202
20 Chen M, Ren B B, Wu Q X, et al. Anti-disturbance control of hypersonic flight vehicles with input saturation using disturbance observer. Sci China Inf Sci, 2015, 58: 070202

21 Chen M, Ge S S. Adaptive neural output feedback control of uncertain nonlinear systems with unknown hysteresis using disturbance observer. IEEE Trans Ind Electron, 2015, 62: 7706–7716
22 Yong K N, Chen M, Wu Q X. Anti-disturbance control for nonlinear systems based on interval observer. IEEE Trans Ind Electron, 2020, 67: 1261–1269
23 Zhu Y K, Guo L, Yu X, et al. An enhanced anti-disturbance control law for systems with multiple disturbances. Sci China Inf Sci, 2020, 63: 209206
24 Astolfi A, Ortega R. Immersion and invariance: a new tool for stabilization and adaptive control of nonlinear systems. IEEE Trans Autom Control, 2003, 48: 590–606
25 Karagiannis D, Carnevale D, Astolfi A. Invariant manifold based reduced-order observer design for nonlinear systems. IEEE Trans Autom Control, 2008, 53: 2602–2614
26 Liu Z, Tan X M, Yuan R Y, et al. Immersion and invariance-based output feedback control of air-breathing hypersonic vehicles. IEEE Trans Autom Sci Eng, 2016, 13: 394–402
27 Astolfi A, Ortega R, Venkatraman A. A globally exponentially convergent immersion and invariance speed observer for mechanical systems with non-holonomic constraints. Automatica, 2010, 46: 182–189
28 Bechlioulis C P, Rovithakis G A. Robust adaptive control of feedback linearizable MIMO nonlinear systems with prescribed performance. IEEE Trans Autom Control, 2008, 53: 2090–2099
29 Bechlioulis C P, Karras G C, Heshmati-Alamdari S, et al. Trajectory tracking with prescribed performance for underactuated underwater vehicles under model uncertainties and external disturbances. IEEE Trans Control Syst Technol, 2017, 25: 429–440
30 Hu Q L, Shao X D, Guo L. Adaptive fault-tolerant attitude tracking control of spacecraft with prescribed performance. IEEE/ASME Trans Mechatron, 2018, 23: 331–341
31 Yong K N, Chen M, Shi Y, et al. Flexible performance-based robust control for a class of nonlinear systems with input saturation. Automatica, 2020, 122: 109268
32 An H, Xia H W, Wang C H. Barrier Lyapunov function-based adaptive control for hypersonic flight vehicles. Nonlinear Dyn, 2017, 88: 1833–1853
33 Liu W K, Wei Y Y, Duan G R. Barrier Lyapunov function-based integrated guidance and control with input saturation and state constraints. Aerospace Sci Tech, 2019, 84: 845–855
34 Shin H S, Tsourdos A, Li K B. A new three-dimensional sliding mode guidance law variation with finite time convergence. IEEE Trans Aerosp Electron Syst, 2017, 53: 2221–2232
35 Beard R W, Ferrin J, Humpherys J. Fixed wing UAV path following in wind with input constraints. IEEE Trans Contr Syst Technol, 2014, 22: 2103–2117
36 Yong K N, Chen M, Shi Y, et al. Hybrid estimation strategy-based anti-disturbance control for nonlinear systems. IEEE Trans Autom Control, 2021, 66: 4910–4917